Ligand Binding in the Ferric and Ferrous States of *Paramecium* Hemoglobin†

Tapan Kanti Das,*,‡ Roy E. Weber,§ Sylvia Dewilde,|| Jonathan B. Wittenberg,‡ Beatrice A. Wittenberg,‡ Kiyoshi Yamauchi,⊥ Marie-Louise Van Hauwaert,|| Luc Moens,|| and Denis L. Rousseau‡

Department of Physiology and Biophysics, Albert Einstein College of Medicine, 1300 Morris Park Avenue, Bronx, New York 10461, Danish Centre for Respiratory Adaptation, Department of Zoophysiology, Institute of Biological Sciences, University of Aarhus, DK-8000 Aarhus C, Denmark, Department of Biochemistry, University of Antwerp, Universiteitsplein 1, B-2610 Antwerp, Belgium, and Department of Biology, Faculty of Science, Shizuoka University, 836 Oya, Shizuoka 422-8529, Japan

Received July 19, 2000

ABSTRACT: The unicellular protozoan *Paramecium caudatum* contains a monomeric hemoglobin (Hb) that has only 116 amino acid residues. This Hb shares the simultaneous presence of a distal E7 glutamine and a B10 tyrosine with several invertebrate Hbs. In the study presented here, we have used ligand binding kinetics and resonance Raman spectroscopy to characterize the effect of the distal pocket residues of *Paramecium* Hb in stabilizing the heme-bound ligands. In the ferric state, the high-spin to low-spin (aquo-hydroxy) transition takes place with a pK_a of ∼9.0. The oxygen affinity (P_{50} = 0.45 Torr) is similar to that of myoglobin. The oxygen on- and off-rates are also similar to those of sperm whale myoglobin. Resonance Raman data suggest hydrogen bonding stabilization of bound oxygen, evidenced by a relatively low frequency of Fe−OO stretching (563 cm^{-1}). We propose that the oxy complex is an equilibrium mixture of a hydrogen-bonded closed structure and an open structure. Oxygen will dissociate preferentially from the open structure, and therefore, the fraction of open structure population controls the rate of oxygen dissociation. In the CO complex, the Fe−CO stretching frequency at 493 cm^{-1} suggests an open heme pocket, which is consistent with the higher on- and off-rates for CO relative to those in myoglobin. A high rate of ligand binding is also consistent with the observation of an Fe−histidine stretching frequency at 220 cm^{-1}, indicating the absence of significant proximal strain. We postulate that the function of *Paramecium* Hb is to supply oxygen for cellular oxidative processes.

There has been an increasing growth of interest in understanding the structure, function, and evolution of the invertebrate Hbs[1] because of their diverse cellular locations and unique physical properties. The invertebrate Hbs bind molecular oxygen and other diatomic ligands such as CO and NO just as their vertebrate counterparts; however, the affinity of ligand binding is widely different among the two classes of globins. In comparison to vertebrate globins, the oxygen binding properties of the invertebrate tissue Hbs in many cases makes them unsuitable for intracellular oxygen transport, the classical function of mammalian Mbs. Therefore, a variety of activities of the invertebrate Hbs has been proposed in recent years (*1*−*10*). While our knowledge of the cellular function of these Hbs is only at the level of speculation to date, there has been some progress in determining the structural features at the molecular level via spectroscopic (*10*−*22*) and X-ray crystallographic techniques (*23*−*25*).

The Hb of the unicellular protozoan *Paramecium caudatum* (*26*) is grouped into a special class termed truncated Hbs (∼120 amino acids) (*23*) whose amino acid sequences differ widely from those of mammalian Mb and Hb. The three-dimensional structure of the truncated Hbs displays a two-over-two helical sandwich fold instead of the three-over-three helical sandwich fold of mammalian Hbs and Mbs. *Paramecium* and the green alga *Chlamydomonas eugametos* Hb genes have introns at positions unprecedented in other globin genes, whereas the bacterial Hb genes lack introns (*27*−*29*).

The degree of amino acid sequence similarity of *Paramecium* Hb and mammalian Mb and Hb is very low (15%)

† This work was supported by NIH Grants GM54806 and GM54812 to D.L.R., the Danish Natural Science Research Council (R.E.W.), and FWO-Vlaanderen (Foundation for Scientific Research-Flanders) Grant 3G031400 to L.M. S.D. is a postdoctoral fellow of the FWO.

* To whom correspondence should be addresses. Telephone: (718) 430-2899. Fax: (718) 430-4230. E-mail: tdas@aecom.yu.edu.

‡ Albert Einstein College of Medicine.

§ University of Aarhus.

|| University of Antwerp.

⊥ Shizuoka University.

[1] Abbreviations: Hb, hemoglobin; *Paramecium* Hb, *P. caudatum* hemoglobin; HbO_2, oxyhemoglobin; HbCO, carbon monoxy hemoglobin; Mb, myoglobin; MbO_2, oxymyoglobin; MbCO, carbon monoxy myoglobin; HbA, adult human hemoglobin; CHES, 2-(cyclohexylamino)ethanesulfonic acid; CAPS, 3-(cyclohexylamino)-1-propanesulfonic acid; HEPES, 4-(2-hydroxyethyl)-1-piperazineethanesulfonic acid; Tris, tris(hydroxymethyl)aminomethane; EPPS, 4-(2-hydroxyethyl)-1-piperazinepropanesulfonic acid; MES, 2-morpholinoethanesulfonic acid; Bis-Tris, [bis(2-hydroxyethyl)imino]tris(hydroxymethyl)-methane; ν_{Fe-His}, Fe−His stretching; ν_{Fe-OO}, Fe−O_2 stretching; ν_{Fe-CO}, Fe−CO stretching; ν_{C-O}, C−O stretching; δ_{Fe-C-O}, Fe−C−O bending; k'_{on}, oxygen association rate constant; k_{off}, oxygen dissociation rate constant; K_d, oxygen equilibrium constant; P_{50}, oxygen affinity expressed as half-saturation oxygen tension; n_{50}, Hill's cooperativity coefficient at P_{50}; l'_{on}, CO association rate constant; l_{off}, CO dissociation rate constant; L_d, CO equilibrium constant; M, partition coefficient expressed in gas pressure; M', partition coefficient expressed in a molar term.

10.1021/bi001681d CCC: $19.00
Published on Web 10/27/2000

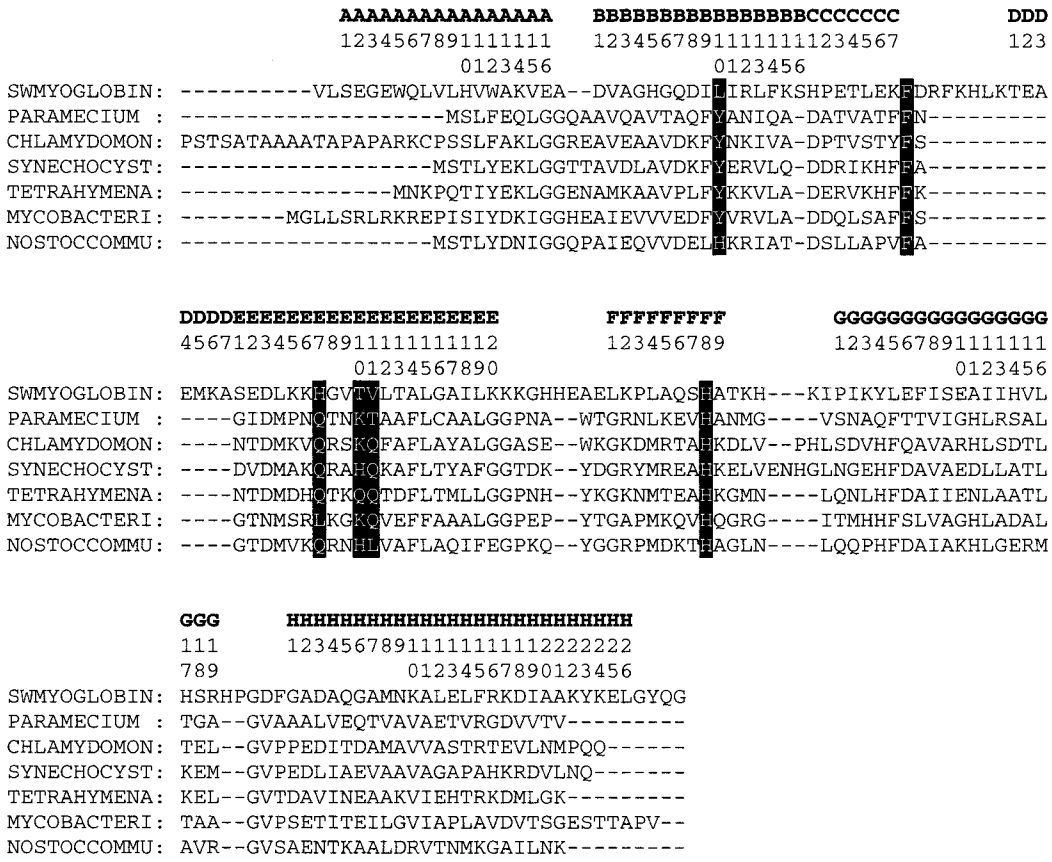

FIGURE 1: Comparison of the amino acid sequence of *P. caudatum* Hb to those of sperm whale myoglobin (SWMYOGLOBIN) and some invertebrate Hbs, including those of *C. eugametos* (CHLAMYDOMON), *Synechocystis* PCC6803 (SYNECHOCYST), *Tetrahymena pyriformis* (TETRAHYMENA), *M. tuberculosis* (MYCOBACTERI), and *Nostoc commune* (NOSTOCCOMMU). Sequence alignment and the calculation of the degree of sequence identity were achieved using Insight II (MSI, San Diego, CA).

(Figure 1). The proximal histidine anchors the heme into the globin cavity as in all Mbs and Hbs. In contrast to the distal E7 histidine of most of the mammalian Mbs, distal positions E7 and B10 of *Paramecium* Hb are occupied by glutamine and tyrosine, respectively (*23*). Although *Paramecium* Hb was isolated and sequenced more than a decade ago (*26*) and had been known to bind oxygen, very little information about its oxygen binding properties at the molecular level is available. In the work presented here, we carried out stopped-flow kinetic and Raman spectroscopic investigations to decipher the oxygen binding of recombinant *Paramecium* Hb, expressed in *Escherichia coli*. Soret-enhanced resonance Raman spectroscopy is known to be an extremely useful technique in studying heme proteins. We present results of resonance Raman measurements with the oxy and the CO forms of *Paramecium* Hb as well as the kinetics and equilibria of its reactions with O_2 and CO. We also characterize the protein in its ferrous (deoxy) and ferric (aquomet) states to explore the influence of the redox state on the heme pocket dynamics. The spectroscopic and kinetic data are discussed in an attempt to elucidate the possible cellular function of this invertebrate Hb.

EXPERIMENTAL PROCEDURES

Construction and Expression of an Artificial P. caudatum Globin cDNA. A synthetic *P. caudatum* cDNA, using the codon frequency of *E. coli*, was constructed from 15 oligonucleotides essentially according to the method of Ikehara et al. (*30*). The synthetic globin gene was designed to be 0.36 kb long with an *Nde*I site at the 5′ end and a *Bam*HI site at the 3′ end. It was ligated into the corresponding restriction sites of pET3a to create the *P. caudatum* globin expression plasmid, pPc-HB. The correctness of the construct was verified by dideoxy sequencing.

The expression plasmid was transformed in *E. coli* strain BL21(DE3)pLysS, and the cells were grown at 25 °C in LB medium containing 300 μg/mL ampicillin, 30 μg/mL chloramphenicol, and 1 mM δ-aminolevulinic acid. The culture was induced at an A_{600} of 0.8 by addition of isopropyl 1-thio-β-D-galactopyranoside to a final concentration of 0.4 mM, and expression was continued overnight. Cells were harvested, washed, and resuspended in lysis buffer [50 mM Tris-HCl (pH 8), 1 mM EDTA, and 0.5 mM dithiothreitol]. The cells were then exposed to three freeze−thaw steps and were sonicated until they were completely lysed (*31*).

P. caudatum Hb was purified from the total lysate by ammonium sulfate precipitation (40 and 80%), by two cycles of DEAE fast flow chromatography (Pharmacia) (step and gradient elution), and finally by gel filtration on a Superdex 75 column (Pharmacia). The purity of the fractions was monitored by SDS−PAGE. Two milligrams of pure *P. caudatum* Hb was obtained per liter of medium.

Equilibrium Measurements of the Level of Oxygen Binding. Oxygen equilibria were assessed at 5, 15, and 25 °C using a modified gas diffusion chamber technique (*32*, *33*), where thin layers of Hb solutions, whose absorbances are

continuously monitored, are equilibrated with oxygen, ultrapure (>99.998%) nitrogen, and gas mixtures with stepwise-increased oxygen tensions, delivered by cascaded Wösthoff gas mixing pumps (Bochum, Germany). pH values in the Hb solutions were varied using Tris or bisTris/MES buffers (final concentration of 0.1 M) and were measured at the same temperature as the oxygen equilibrium measurements were carried out, using a BMS Mk2 thermostated electrode (Radiometer, Copenhagen, Denmark). The overall heat of oxygenation was calculated from the van't Hoff equation $\Delta H' = [2.303R(\Delta \log P_{50})]/(1/T_1 - 1/T_2)$, where T_1 and T_2 are absolute temperatures and R is the gas constant.

Ligand Reaction Rates. These were measured at 20 °C as previously described (*12*, *34*). The buffer that was used was 50 mM potassium or sodium HEPES (pH 7.5) containing 50 μM EDTA.

Oxygen Dissociation Rates. Solutions of *Paramecium* HbO_2 (5 μM HbO_2; 1350 μM oxygen in buffer) were mixed rapidly with solutions of carbon monoxide (1000 μM in buffer containing 1 mM dithionite), and the reaction was followed at 422 and 411 nm, a maximum and a minimum, respectively, in the HbCO minus HbO_2 difference spectrum.

Carbon Monoxide Combination Rate. Solutions of *Paramecium* deoxy-Hb (3 μM heme in buffer containing 1 mM sodium dithionite) were mixed rapidly with solutions of CO (12.5−50 μM in buffer containing 1 mM sodium dithionite), and the reaction was followed at 420 and 435 nm, a maximum and a minimum, respectively, in the HbCO minus deoxyHb difference spectrum. The observed kinetic events were homogeneously single-exponential. The second-order combination rate constant was obtained graphically as the slope of the relation of the observed rate to the ligand concentration (after mixing).

Carbon Monoxide Dissociation Rate. Solutions of *Paramecium* HbCO (5 μM HbCO, 50 nM free CO in buffer containing 1 mM dithionite) were mixed rapidly with a saturated solution of *n*-butyl isocyanide (Sigma-Aldrich) in buffer containing 1 mM dithionite, and the reaction was followed at 422 and 434 nm, wavelengths close to the minimum and maximum, respectively, in the *n*-butyl isocyanide minus CO difference spectrum of the protein. Dithionite is known not to interfere in this reaction (*35*). Nearly homogeneous first-order kinetic events were observed with 75−90% of the expected absorption change observed at each wavelength.

Partition of Paramecium Hb between Oxygen and Carbon Monoxide. The partition coefficient was determined at a total gas pressure of 1 atm as described previously (*12*). Calculations were carried out from the sum of absorbance changes at 408 and 422 nm, a minimum and a maximum, respectively, in the HbCO minus HbO_2 difference spectrum.

Resonance Raman Spectroscopy. The Raman experiments were carried out with 413.1 nm excitation from a CW Kr-ion laser (Spectra Physics, Mountain View, CA). The sample cell (quartz, 2 mm path length, sample volume of ~150 μL), into which a laser beam was focused, was spun at 6000 rpm to minimize local heating. The sample cells are custom designed for strict anaerobic measurements and can be used for recording both the resonance Raman spectra and the optical absorption spectra (UV-2100U spectrophotometer, Shimadzu, Kyoto, Japan). The Raman scattered light was focused onto the entrance slit (100 μm) of a polychromator (Spex, Metuchen, NJ), dispersed by a 1200 grooves/mm grating and detected by a liquid nitrogen-cooled charged couple device (CCD) (Princeton Instruments, Trenton, NJ). A holographic notch filter (Kaiser, Ann Arbor, MI) was used to eliminate Rayleigh scattering. Typically, several 30 s spectra were recorded and averaged. Frequency shifts in the Raman spectra were calibrated using an acetone/CCl_4 mixture (for the 100−1000 cm^{-1} region), indene (for the 100−1700 cm^{-1} region), and an acetone/ferrocyanide mixture (for the 1700−2300 cm^{-1} region) as references. The accuracy of the Raman shifts is about ± 1 cm^{-1} for absolute shifts and about ± 0.25 cm^{-1} for relative shifts. The Raman data were processed by using GRAMS (Galactic Industries Corp.) software. The cosmic ray spikes were removed by using CSMA subroutines (Princeton Instruments).

The concentration of protein samples used for the Raman measurements was typically 40 μM in 100 mM buffer. For deoxy samples, *Paramecium* Hb was reduced by the addition of a freshly prepared dithionite solution to the degassed protein solution under anaerobic conditions. HbCO was prepared by exposing dithionite-reduced samples to either $^{12}C^{16}O$ or $^{13}C^{18}O$ in tightly sealed Raman cells. $^{13}C^{18}O$ gas was a product of ICON (Mt. Marion, NY), and $^{12}C^{16}O$ was obtained from Matheson (Rutherford, NJ). The laser power was maintained at ~0.5 mW at the sample to minimize carbon monoxide dissociation. Absorption spectra were recorded before and after the Raman measurements to ensure the stability of the species that were being studied. For the oxy samples (with $^{16}O_2$ and $^{18}O_2$), the power of the laser beam used at the sample was ~1 mW. To obtain freshly prepared HbO_2, an aliquot of the CO complex was saturated with 1 atm O_2 by passing ultrapure oxygen gas over the protein solution for 1 h. The CO complex was made by passing the protein solution, preincubated with dithionite and CO, through a Sephadex G-25 column (40 mM EPPS, pH 7.4). Solutions of *Paramecium* HbO_2 in two isotopic compositions of water were prepared as follows: 40 μM protein (40 mM sodium phosphate or EPPS, pH 7.4) in 80% D_2O (using 99.9% D_2O, Aldrich Chemical Co. Inc., Madison, WI) and 20 or 100% H_2O. The ferric protein was prepared by oxidizing the oxy form with ferricyanide followed by filtration through a Sephadex G-25 column. Solutions of ferric Hb (40 μM) were prepared in buffers with different pH values: sodium phosphate (pH 6.0−7.4), Tris (pH 8.0−8.5), CHES (pH 9.0−10.0), and CAPS (pH 10.5−11.0).

RESULTS

Optical Spectra. The deoxy form of *Paramecium* Hb exhibits absorbance maxima at 432 and ~560 nm (Figure 2), typical of high-spin ferrous Hb and Mb (*36*). In the oxy complex of *Paramecium* Hb the Q-bands at 543 and 580 nm are similar to those of sperm whale MbO_2, but the Soret band is slightly blue-shifted to 415 nm. The CO complex of *Paramecium* Hb has a position of the Soret band (422 nm) similar to that in MbCO, but the α-band at 567 nm differs significantly from that of MbCO (579 nm) (*36*). The ferric protein undergoes an acid−alkaline transition from a high-spin species (407, 503, and 633 nm) at pH 7.5 to a low-spin species (410 and 543 nm) at pH 10.5.

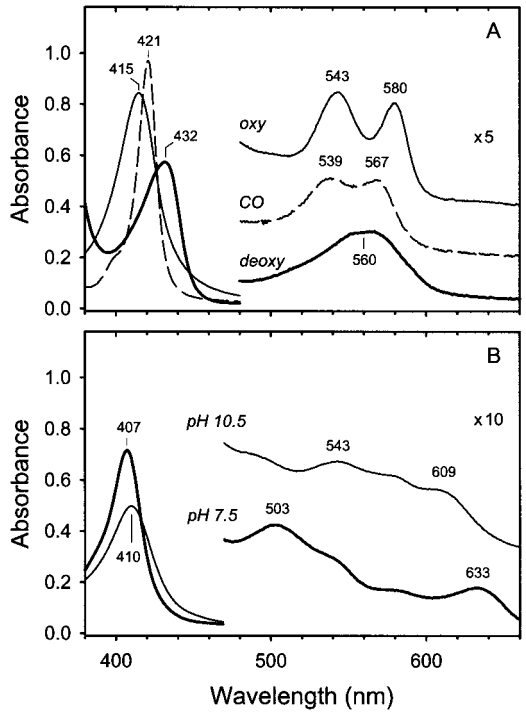

FIGURE 2: (A) Optical spectra of the oxy (thin line), CO (dashed line), and deoxy (thick line) complexes of *Paramecium* Hb (pH 7.5). In the visible region spectrum of deoxy Hb, two bands at 551 and 571 nm could be seen easily in the second-derivative spectrum. The midpoint at 560 nm is marked here. (B) Optical spectra of the ferric protein at pH 7.5 (thick line) and 10.5 (thin line). The visible region spectra (470−660 nm) are expanded (5-fold on the *y*-axis in graph A and 10-fold on the *y*-axis in graph B) and vertically displaced for better clarity.

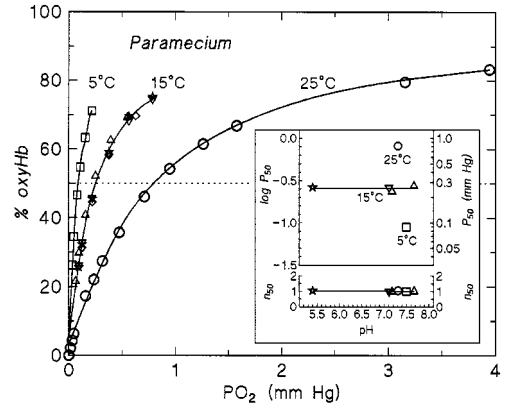

FIGURE 3: O_2 equilibrium curves of *Paramecium* Hb at 5 (□), 15 (△, ▽, ◇, and ☆), and 25 °C (○) measured in 0.1 M Tris (○, △, and ◇), bisTris (▽), and bisTris/MES (☆) buffers. The heme concentration was 0.49 mM. The inset shows the pH dependence of the P_{50} and n_{50} values, showing the absence of cooperativity (n = 1.0) and Bohr effect ($\Delta \log P_{50}/\Delta pH = -0.007$).

Equilibrium Oxygen Binding. Paramecium Hb binds oxygen reversibly and noncooperatively (Figure 3). Values of P_{50} obtained at 5, 15, and 25 °C are 0.089, 0.27, and 0.81 mmHg (Torr), respectively. The value interpolated for 20 °C and 0.45 mmHg corresponds to a dissolved oxygen concentration of 838 nM. The P_{50} value measured here is in agreement with that (0.6 Torr) of an early determination by Smith et al. (*37*).

The oxygen affinity is independent of pH from 6.5 to 8.0, indicating the absence of a Bohr effect (Figure 3B). The

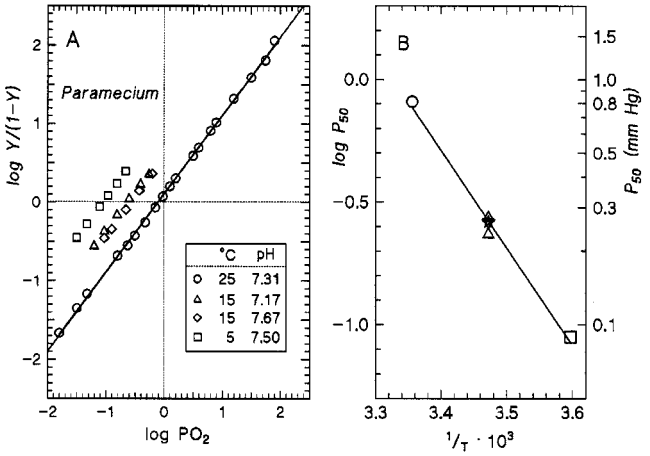

FIGURE 4: Hill plots of the oxygen equilibria (A) showing the absence of oxygenation-linked transitions over a wide range of oxygen saturation (2−99% at 25 °C) and a van't Hoff plot (B) showing the overall heat of oxygenation ($\Delta H'$) of −76 kJ/mol, derived from the linear regression $\log P_{50} = -3.968(1000/T) + 13.201$ ($r = -0.9953$), where T is the absolute temperature.

slopes of the Hill plots of *Paramecium* Hb, determined over a wide range of oxygen saturations and at different pH values, are all unity; the Hill's coefficient $n = 1$ (Figure 4A). This shows that oxygen binding is not cooperative, as expected for the monomeric structure.

The van't Hoff relation (Figure 4B) demonstrates an overall heat of oxygenation, $\Delta H'$, of −76 kJ/mol of O_2 bound. This value is close to those for mammalian Mbs (including sperm whale Mb, $\Delta H' = -80$ kJ/mol; *36*, *38*). These values, which include the heat of solution of oxygen, are high compared to those observed in tetrameric Hbs, where low values result from oxygenation-linked endothermic dissociation of effector ions (protons, chlorides, and organic phosphates). The high value in *Paramecium* Hb is consistent with the absence of oxygenation-linked reactions with effector ions.

O_2 Kinetics. A single homogeneous kinetic event, independent of the observation wavelength, was recorded for replacement of bound oxygen by CO. The dissociation rate (k_{off}) was 25.2 s^{-1} (Table 1). The second-order oxygen combination rate constant could not be measured directly because of competing reactions. The calculated value of the combination rate constant (k'_{on}) for O_2 (see below) is 30.1 μM^{-1} s^{-1}. Both the on- and off-rates are similar to those of sperm whale Mb (Table 1).

CO Kinetics. The CO dissociation rate, determined using *n*-butyl isocyanide as the replacing ligand, exhibits nearly homogeneous first-order kinetics ($l_{off} = 0.328$ s^{-1}, $n = 10$) for the dissociation of CO at 20 °C and pH 7.5. Dissociation of CO in *Paramecium* Hb is 20-fold faster than that in sperm whale Mb (Table 1).

A homogeneous pseudo-first-order kinetic event was observed in the combination of CO with *Paramecium* Hb. The rate constant (l'_{on}) was 27.7 μM^{-1} s^{-1}. The CO affinity, L_D, was calculated as l_{off}/l'_{on} (11.8 nM) (Table 1).

Partitioning of Paramecium Hb between O_2 and CO. The partition coefficient expresses the relative affinity of the protein for carbon monoxide and oxygen. A plot of the [HbCO]/[HbO_2] ratio against the pCO/pO_2 ratio was linear over the range that was examined (Figure 5). The partition coefficient, M, given by the slope of this relation, is 56. This

Table 1: Kinetics and Equilibrium Constants for the Reactions of Ferrous Wild-Type *Paramecium* Hb with Oxygen and Carbon Monoxide Compared to Those of Other Wild-Type Proteins

organism (residues at positions E7 and B10)[a]	oxygen				carbon monoxide			M'
	k'_{on} (μM^{-1} s^{-1})	k_{off} (s^{-1})	K_d (k_{off}/k'_{on}) (nM)	P_{50} (mmHg)	l'_{on} (μM^{-1} s^{-1})	l_{off} (s^{-1})	L_d (l_{off}/l'_{on}) (nM)	K_d/L_d
Paramecium[b] (Q/Y)	30.1	25.2	838	0.45	27.7	0.328	11.8	75
barley[c] (H/F)	7.1	0.0272	3.82	−	0.57	0.0011	1.93	2.0
C. eugametos[d] (Q/Y)	#	0.0141	−	−	#	0.0022	−	5.0
Ascaris[e] (Q/Y)	1.5	0.0041	2.7	0.0038	17	0.018	1.1	2.5
soybean Lba[f] (H/Y)	120	5.6	48	−	13	0.0078	0.62	78
N. commune[g] (Q/H)	390	79	203	0.55	41	0.01	0.24	867
sperm whale Mb[h] (H/L)	14	12	857	0.51	0.51	0.019	37	23
rice Hb1[i] (H/F)	68	0.038	0.56	−	7.2	0.001	0.14	4.0
α-HbA (R)[j] (H/L)	29	10.1	348		3.2	0.0047	1.47	−
β-HbA (R)[j] (H/L)	100	21	210		9.8	0.0086	0.877	−
M. tuberculosis[k] (L/Y)	25	0.199	−	0.013	6.75	0.0051	−	7.44
Paramphistomum epiclitum[l] (Y/Y)	108	0.033	0.3	0.00016	28	−	−	−
Gastrothylax crumenifer[l] (Y/Y)	205	0.4	1.9	0.001	73	1.2	16	0.119
Arabidopsis thaliana Hb1[m] (H/F)	−	0.12	1.6	−	−	−	−	2.0
Lucina Hb II[n] (Q/Y)	0.39	0.11	282	0.13	0.019	0.0071	370	−

[a] The residues at putative E7 and B10 helical positions are given in parentheses. The value of k'_{on} is calculated; see the text. The P_{50} value is in units of millimeters of Hg (Torr). $M' = 1.34M$, where M is the experimentally determined value of the partition coefficient expressed in terms of gas pressures. M' for other proteins is given by the ratio K_d/L_d. [b] *P. caudatum* Hb, this work. [c] From ref *34*, k'_{on} is estimated from M', k_{off}, and L_d. [d] *C. eugametos* Hb (*12*), data obtained at pH 9.5. The # symbols show that combination rates of five-coordinate *Chlamydomonas* Hb with ligands are rate limited by the conversion of a six-coordinate species to a five-coordinate species prior to ligand binding (see the details in ref *12*). [e] From ref *71*. [f] From ref *72*. [g] *N. commune* Hb (*14*). [h] Sperm whale Mb (*73*). [i] From ref *56*. [j] From ref *74*, α and β chains of HbA in their R states. [k] *M. tuberculosis* HbN (*18*). [l] *P. epiclitum* Hb, *G. crumenifer* Hb (see refs *53* and *75*, respectively). [m] *A. thaliana* Hb1 (*76*). [n] *L. pectinata* Hb (*21*).

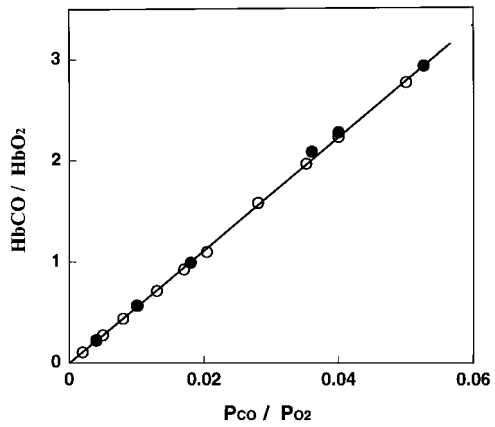

FIGURE 5: Plot of [HbCO]/[HbO_2] vs P_{CO}/P_{O_2}. The partition coefficient M (expressed in gas pressures) = 56, and M' (expressed in molar terms) = 75. Different symbols denote data points from two separate experiments.

value is expressed in terms of the gaseous pressures. A value, M', corrected for the solubility of the gases and expressed in molar terms, is related to M by $M' = 1.34M = 75$ (Table 1).

Calculated Kinetic and Equilibrium Constants. The partition coefficient, M', calculated from the determined oxygen equilibrium binding constant, K_D, and the calculated CO equilibrium binding constant, L_D (Table 1), is K_D/L_D (838 nM/11.8 nM = 71). This value agrees with the determined value, 75.

A value of the second-order oxygen combination rate constant (k'_{on}, Table 1) may be calculated using the determined oxygen equilibrium binding constant, K_D, and the determined oxygen dissociation rate constant: $k_{off}/K_D = 25.2$ $s^{-1}/0.838$ $\mu M = 30.1$ μM^{-1} s^{-1}. Alternatively, the combination rate constant, k'_{on}, may be estimated from the determined value of the partition coefficient, M', and the values of the three kinetic constants, k_{off}, l'_{on}, and l_{off}. This latter value, 28.4 μM^{-1} s^{-1}, is in good agreement with the value mentioned above, 30.1 μM^{-1} s^{-1}.

We conclude that the set of determined values is internally consistent and that the value of the calculated oxygen combination rate constant ($k'_{on} = 30.1$ μM^{-1} s^{-1}) is accurate.

Resonance Raman Spectra of the Deoxy Complex. The high-frequency region (1300−1700 cm^{-1}) of the resonance Raman spectra of hemeproteins is comprised of porphyrin in-plane vibrational modes that are sensitive to the electron density in the porphyrin macrocycle and also to the oxidation, coordination, and spin state of the central iron atom (*39*). The spectrum in the high-frequency region of the deoxy form of *Paramecium* Hb shows the marker bands ($\nu_4 = 1355$ cm^{-1}, $\nu_3 = 1473$ cm^{-1}) characteristic of five-coordinate high-spin ferrous heme (Figure 6A). The deoxy forms of vertebrate Hbs and Mbs exhibit very similar resonance Raman spectra. Thus, in *Paramecium* deoxyHb, in contrast to the six-coordinate low-spin ferrous forms of some invertebrate Hbs (*11*, *12*), no intrinsic sixth ligand binds the ferrous heme iron.

The low-frequency region of resonance Raman spectra of heme proteins is comprised of several in-plane and out-of-plane vibrational modes of the heme, including heme propionate modes and ligand vibrational modes (*40*−*43*). Enhancement of the vibrational modes involving the axial ligand (bound to the central metal atom) arises from electronic coupling of the ligand orbitals to the heme orbitals. Assignment of a ligand vibrational mode is extremely useful as it directly identifies a particular ligand and the nature of its interactions with amino acid residues in the heme pocket. The low-frequency region of the resonance Raman spectrum of *Paramecium* deoxyHb (Figure 6B) shows several in-plane skeletal modes ($\nu_8 = 350$ cm^{-1}, $\nu_7 = 676$ cm^{-1}, $\nu_{15} = 755$ cm^{-1}, and $\nu_6 = 785$ cm^{-1}) similar to those observed in deoxyMb (*39*). Bending modes sensitive to the conformation of propionate ($\delta_{C\beta CcCd} = 375$ cm^{-1}) and vinyl ($\delta_{C\beta CaCb} = 405$ cm^{-1}) groups of the protoheme are also assigned (*39*).

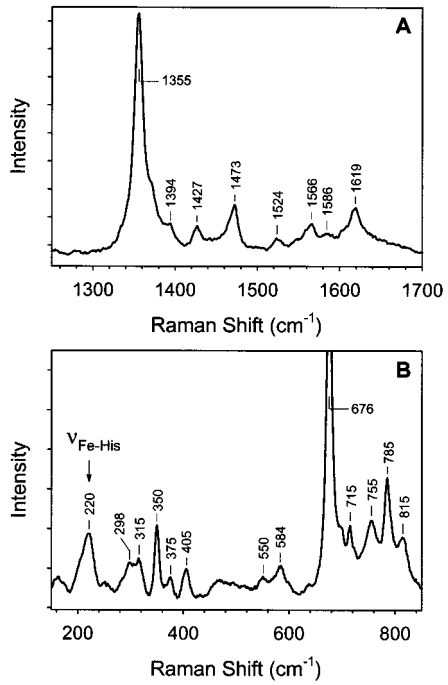

FIGURE 6: Resonance Raman spectra of the deoxy ferrous *Paramecium* Hb (pH 7.4) in the high (A)- and low-frequency (B) regions. The Fe−histidine stretching mode is indicated with an arrow.

Of particular interest is the band at 220 cm^{-1} that is assigned as the Fe−His (proximal) stretching mode (ν_{Fe-His}). The low-frequency ν_{Fe-His} band in five-coordinate high-spin ferrous hemes (other than in some peroxidases) occurs between 200 and 230 cm^{-1} (*41*, *42*, *44*−*46*). Observation of a line that can be attributed to the Fe−His stretching frequency confirms that histidine is the proximal ligand to the heme in *Paramecium* Hb.

Oxy Complex. The oxy complex of *Paramecium* Hb shows a typical six-coordinate low-spin structure of the heme as determined from the resonance Raman marker bands (ν_4 = 1375 cm^{-1}, ν_3 = 1505 cm^{-1}). The oxy samples that were not stored under saturating oxygen pressure showed rapid autoxidation (*47*) to form an aquomet structure which is identified by the presence of a band in the Raman spectrum at 1480 cm^{-1} that can be assigned to the ν_3 of the ferric six-coordinate high-spin aquomet species. In the oxy complex, the location of the oxidation state marker (ν_4) and the spin state marker (ν_3) bands at 1375 and 1505 cm^{-1}, respectively, which are typical for low-spin ferric heme, is consistent with a low-spin ferric superoxide structure ($Fe^{3+}-O-O^{-}$) rather than a ferrous oxy ($Fe^{2+}-O{=}O$) structure. Similar frequencies of ν_3 and ν_4 are observed in the oxy complex of other Hbs and Mbs.

The assignment of the stretching frequency of $Fe-O_2$ (ν_{Fe-OO}) confirmed by using isotopically labeled molecular oxygen ($^{16}O_2$ and $^{18}O_2$) is shown in Figure 7. The broad band in the absolute spectrum at 558 cm^{-1} with $^{16}O_2$ (spectrum a) shifts to 547 cm^{-1} with $^{18}O_2$ (spectrum b), showing a shift of only 11 cm^{-1} in contrast to the expected shift of ∼20 cm^{-1} for the $Fe-O_2$ system. However, observation of a clean symmetric difference spectrum at 563/540 cm^{-1} (spectrum c) with a frequency shift of 23 cm^{-1} indicates that some porphyrin internal modes overlap (*48*) with the position of ν_{Fe-OO}. Thus, the frequency of ν_{Fe-OO} is assigned at 563 cm^{-1}

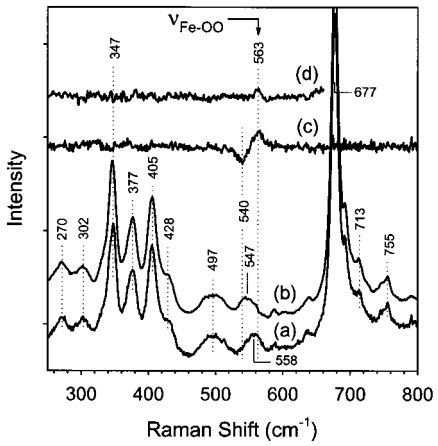

FIGURE 7: Resonance Raman spectra of the oxy complex of *Paramecium* Hb (pH 7.4) in the low-frequency region. The spectra shown are (a) with $^{16}O_2$, (b) with $^{18}O_2$, (c) the $^{16}O_2$ − $^{18}O_2$ difference, and (d) the H_2O − D_2O difference with $^{16}O_2$. The Fe−oxygen stretching mode (ν_{Fe-OO}) is indicated with an arrow.

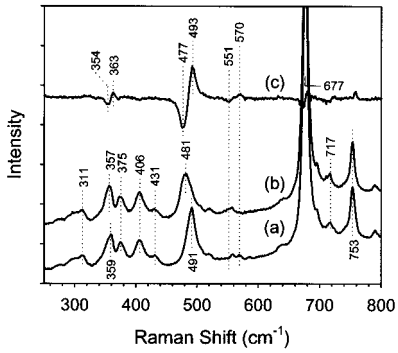

FIGURE 8: Resonance Raman spectra of the carbon monoxide complex of *Paramecium* Hb (pH 7.4) in the low-frequency region. The spectra shown are (a) with $^{12}C^{16}O$, (b) with $^{13}C^{18}O$, and (c) the $^{12}C^{16}O$ − $^{13}C^{18}O$ difference. The Fe−CO stretching (ν_{Fe-OO}) and Fe−C−O bending (δ_{Fe-C-O}) modes are assigned at 493 and 570 cm^{-1}, respectively.

(ν_{Fe-OO} = 540 cm^{-1} with $^{18}O_2$). The sensitivity of the ν_{Fe-OO} mode to H/D exchange was also examined, shown in spectrum d. A positive band at 563 cm^{-1}, albeit weak, is reproducibly seen in the difference spectrum which arises due to a small decrease in the intensity of ν_{Fe-OO} in D_2O relative to that in H_2O.

CO Complex. The resonance Raman spectrum of the CO complex of *Paramecium* Hb was recorded at a low laser power to avoid photodissociation. A six-coordinate low-spin configuration characterized by frequencies ν_4 (1369 cm^{-1}) and ν_3 (1496 cm^{-1}) is observed. The absence of bands at ∼1355 (ν_4) and ∼1473 (ν_3) cm^{-1} (corresponding to a five-coordinate ferrous heme) in the spectrum indicates that no detectable photodissociation occurs.

The Fe−CO stretching mode (ν_{Fe-CO}) has been identified in the CO complexes of many heme proteins. Its frequency is sensitive to interactions of the bound CO with neighboring residues. Figure 8B shows the low-frequency region spectra of the CO derivative of *Paramecium* Hb with two isotopic compositions of the bound CO. In the difference spectrum ($^{12}C^{16}O$ − $^{13}C^{18}O$, spectrum c), the 493/477 cm^{-1} feature is assigned to the Fe−CO stretching frequency while the weak feature at 570/551 cm^{-1} is assigned to the bending mode (δ_{Fe-C-O}). The third difference feature at 363/354 cm^{-1} that

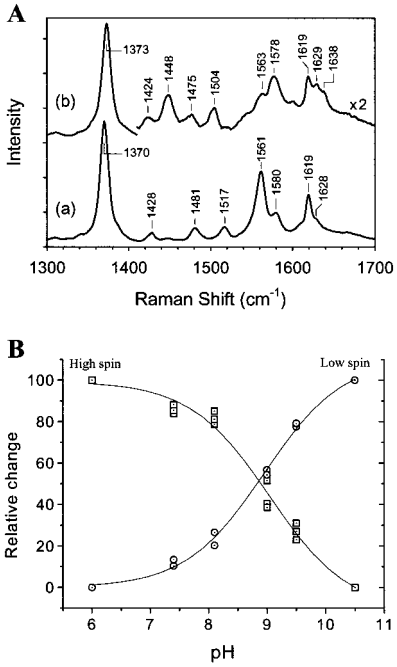

FIGURE 9: (A) Resonance Raman spectra of the ferric aquomet form of *Paramecium* Hb in the high-frequency region at (a) pH 6.0 and (b) pH 10.5. (B) The acid−alkaline transition of *Paramecium* Hb. Relative changes in the high- and low-spin contents are plotted as a function of pH. The relative spin contents are determined from the intensity of several marker bands (normalized to the intensity of ν_4).

arises from an apparent frequency shift of a porphyrin internal mode (ν_8 at 359 cm^{-1}) involving Fe−pyrrole nitrogen stretching could not be assigned to any FeCO-related mode.

Ferric Aquomet Complex. Figure 9A shows the resonance Raman spectra of ferric *Paramecium* Hb in the high-frequency region at two pH values. At acidic pH (6.0), a six-coordinate high-spin species ($\nu_4 = 1370$ cm^{-1}, $\nu_3 = 1481$ cm^{-1}; spectrum a) (*49*) is observed. It is converted to a six-coordinate low-spin species ($\nu_4 = 1373$ cm^{-1}, $\nu_3 = 1505$ cm^{-1}; spectrum b) at alkaline pH (10.5). The presence of an oxygenic ligand (water or hydroxide) bound to the ferric heme iron has been observed in the crystal structure of *Paramecium* Hb (*23*). Thus, the spin transition observed here is most likely an aquo−hydroxy transition. A plot (Figure 9B) of the relative populations of the high- and low-spin species as a function of pH yields the pK_a of the acid−alkaline transition as 9.0 ± 0.3. This value of the pK_a may be compared to the pK_a (8.9) of an alkaline transition of metMb (*36*).

DISCUSSION

Equilibrium Oxygen Binding. Monomeric cytoplasmic Hbs and Mbs exhibit a large variation in oxygen affinities. *Paramecium* Hb exhibits a moderate oxygen affinity, similar to that of sperm whale Mb but different from the extremely high affinities of many truncated Hbs (Table 1) and of nematode, trematode, and other nonvertebrate Hbs and Mbs (*50*−*55*).

Ferric Paramecium Hb. In the ferric form of *Paramecium* Hb, we postulate that a water or a hydroxide ligand binds to the heme, just as in vertebrate metMb and metHb. Both optical and resonance Raman spectra are in accord with this proposal. In a growing number of invertebrate, plant, and bacterial Hbs, however, the heme iron binds to one of the distal pocket residues to form a six-coordinate low-spin species, in the absence of a stronger exogenous ligand (*10*, *11*, *34*, *56*). These latter Hbs undergo significant structural changes in going from an intrinsic ligand-bound state to an exogenous ligand-bound state. It is likely that such structural changes do not occur in ferric *Paramecium* Hb as they are not required for the change from the aquomet to the hydroxymet configuration.

Deoxy Complex. The deoxy form of *Paramecium* Hb is a five-coordinate high-spin species evidenced from the optical as well as the resonance Raman spectra. The ν_{Fe-His} frequency of *Paramecium* Hb is seen at 220 cm^{-1} similar to those in Mb and R-state human Hb (HbA). It is known that the frequency of ν_{Fe-His} in deoxy HbA is responsive to both the quaternary state of the protein and the history of the ligation state of the heme immediately prior to the measurement. The frequency of ν_{Fe-His} increases on going from the T to the R state. There are bounded ranges for the frequency of ν_{Fe-His} for each tertiary and quaternary state of Hb. The frequencies of deoxy T and deoxy R states are observed at ∼214 and ∼222 cm^{-1}, respectively (*41*, *42*, *45*, *46*). In these states, the frequency of ν_{Fe-His} has been correlated with proximal strain (*41*, *42*, *45*, *57*, *58*). Proximal strain refers to the protein-imposed cost in energy needed to move the iron in plane upon ligand binding. A low frequency for ν_{Fe-His} for the five-coordinate ferrous Hb (e.g., deoxyHbA T state) indicates that it is energetically more costly to bind a ligand to this species than to the deoxyHbA R state and deoxyMb ($\nu_{Fe-His} \sim 220$ cm^{-1}). Thus, an R-state-like frequency of ν_{Fe-His} in *Paramecium* Hb suggests a relatively unstrained proximal histidine, indicative of higher ligand affinity (association rate). The association rate for O_2 in *Paramecium* Hb (30.1 μM^{-1} s^{-1}) indeed is similar to those observed for the R state of the α- and β-chains of HbA and for sperm whale Mb (Table 1). The association rate of CO in *Paramecium* Hb, however, is significantly higher than those in Mb and the R state of α-HbA, suggesting an additional contributing factor, namely, "openness" of the distal pocket, determining the CO affinity, which will be discussed in the following sections.

To determine the protonation state of the proximal histidine in *Paramecium* Hb, we compare its ν_{Fe-His} frequency to those in peroxidases. It is believed that the origin of the anomalously high frequency of ν_{Fe-His} in peroxidases is in part due to the imidazolate character of the proximal histidine (*41*, *43*). In peroxidases, the ν_{Fe-His} mode is detected at a significantly higher frequency (>240 cm^{-1}) compared to those in globins (200−230 cm^{-1}). Consideration of the facts presented here suggests that *Paramecium* Hb, in which the frequency of the ν_{Fe-His} mode is similar to that of mammalian Hbs and Mbs, has an uncharged proximal imidazole (histidine) and not an imidazolate.

Oxy Complex. Both the optical and resonance Raman spectra show that the oxy complex of *Paramecium* Hb is a six-coordinate low-spin species. The ν_{Fe-OO} mode in *Paramecium* HbO_2 appears at a lower frequency (563 cm^{-1}) than that in other globins containing an axial histidine ligand. For example, the $^{16}O_2/^{18}O_2$ difference features of human HbO_2 and horse MbO_2 appear at 568/544 and 571/545 cm^{-1} (*48*), respectively, and that of *Mycobacterium tuberculosis* (HbN)

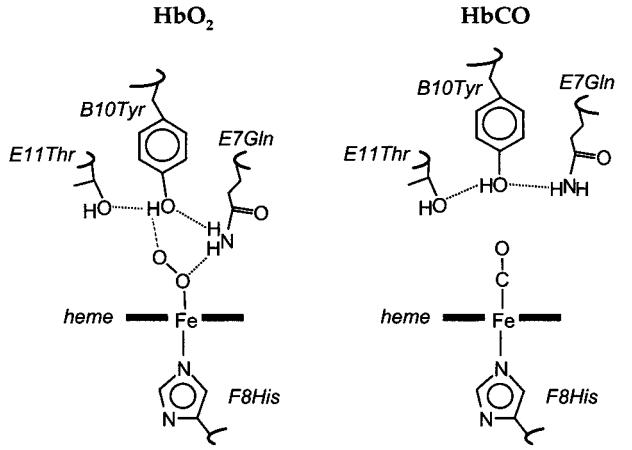

FIGURE 10: Proposed structural model of the disposition of various residues in the heme pocket of the oxy (HbO_2) and CO (HbCO) complexes of *Paramecium* Hb. The residues are numbered according to their helical positions. The dotted and dashed lines represent hydrogen bonds. The thin dashed line between the terminal oxygen atom and the tyrosine hydroxyl indicates a weaker hydrogen bond. For the oxy complex, only the closed conformer is shown here.

HbO_2 is seen at 566/542 cm^{-1} (*18*). In the case of *M. tuberculosis* HbO_2 that has an E7-Leu incapable of forming hydrogen bond to the bound oxygen, it was postulated that the B10-Tyr forms a hydrogen bond to the proximal oxygen atom (*18*, *59*). We attribute the lowering of the ν_{Fe-OO} frequency in *Paramecium* HbO_2 relative to mammalian HbO_2 and MbO_2 to hydrogen bonding of heme distal pocket residues to both the proximal (the oxygen atom bonded directly to iron) and terminal oxygen atoms of the O−O group. This differs from the hydrogen bonding in mammalian HbO_2 and MbO_2 in which only the terminal oxygen atom forms a hydrogen bond to the E7 residue. Hydrogen bond formation to the terminal oxygen alone would not be sufficient to account for the observed low frequency of ν_{Fe-OO} in *Paramecium* Hb. It appears that in *Paramecium* HbO_2 the strength of the hydrogen bond is greater with the proximal oxygen than that with the terminal one (see Figure 10). This suggestion is consistent with significant lowering of the ν_{Fe-OO} frequency as well as the observation of H/D sensitivity of ν_{Fe-OO}.

Our observation of the equilibrium structure of the oxy complex having a relatively tight conformation of the distal pocket predicts slow oxygen dissociation. However, if the protein allows an alternate conformation of the heme pocket, the observed rate of ligand dissociation might be dictated by the structural properties of the second conformer. Such a mechanism has been proposed in the CO complex of *Ascaris* Hb in which a rigid conformer formed by hydrogen bonding from both B10-tyrosine and E7-glutamine remains in equilibrium with a relatively less tight conformer formed by hydrogen bonding with the glutamine alone (*15*). Ligand dissociation is primarily controlled by the latter conformer. We propose that in *Paramecium* Hb a second conformer is in rapid equilibrium with the major conformer that is detected by resonance Raman spectroscopy.

$$Fe-O_2\ (closed) \leftrightarrows Fe-O_2\ (open) \rightarrow Fe^{2+} + O_2$$

In *Paramecium* Hb, perhaps the second conformer in the oxy complex has a more open distal pocket just as we find in the structure of its CO complex (see below). On the other hand, in Mb, the distal pocket attains closed structures for the CO (*60*) as well as the oxy complexes in which the bound ligands form a hydrogen bond with E7-His. Of course at acidic pH the distal cavity of Mb is known to undergo a closed−open transition when the distal histidine swings out of the pocket (*11*, *61*−*63*). The proposed existence of a second conformer with an open heme pocket is consistent with the observed fast rate (25.2 s^{-1}) of oxygen dissociation. Under the experimental conditions used in this study, the second conformer escaped detection in the Raman spectra probably because of its minor population. It will be interesting, however, to search for suitable conditions for enhancing the population of this conformer for its detection.

CO Complex. The CO complex of *Paramecium* Hb is six-coordinate and low-spin, as judged from the optical and resonance Raman spectra. The Fe−CO stretching frequency of *Paramecium* Hb (ν_{Fe-CO} = 493 cm^{-1}) may be compared to those of the Mb mutants in which the distal histidine has been replaced with nonpolar residues. The ν_{Fe-CO} frequencies of these mutants are located at ∼495 cm^{-1} (see ref *64*). Such frequencies of ν_{Fe-CO} are also observed in the A_0 state of Hbs and Mbs at acidic pH and in many other hemeproteins as well, and are believed to arise from an "open" heme pocket where CO has very little polar interaction with surrounding amino acid residues (*11*, *61*−*63*). Thus, the location of ν_{Fe-CO} at 493 cm^{-1} in *Paramecium* Hb suggests that CO does not interact with the distal residues. This is in contrast to the closed form of the oxy protein in which the bound oxygen forms a hydrogen bond with the distal residues. The fact that the iron-bound CO in *Paramecium* Hb does not interact with distal residues is also suggested by the weak Fe−C−O bending mode (570 cm^{-1}). A weak bending mode is normally observed when the heme pocket is open, but a strongly interacting CO gives rise to a more intense bending mode.

The structural model of the CO complex (Figure 10) displays an open heme pocket in which the distal pocket residues barely interact with CO. This is highly consistent with the unusually rapid combination and dissociation of CO with *Paramecium* Hb (l'_{on} and l_{off} are, respectively, 54 and 17 times greater than those of Mb; Table 1). It may also be noted that it is the distal effect that explains why the CO affinity of *Paramecium* Hb is higher than that of Mb or R-state α-HbA, despite the fact that they all have a similar proximal strain as discussed earlier.

Correlation between Fe−CO and C−O Stretching Frequencies. It is well established that in heme complexes the Fe−CO and C−O stretching modes follow an inverse correlation owing to π-electron back-donation from the dπ (d_{xz}, d_{yz}) of Fe to the empty π^* orbitals of CO, which results in an increase of the Fe−CO bond order and a concomitant decrease in the C−O bond order (*11*, *15*, *40*, *65*−*67*). The correlation between these two frequencies depends on the nature of the heme proximal ligand, as the electron density in the Fe−proximal ligand bond affects the Fe−CO bond order. The extent of back-bonding from Fe d_π to CO π^* is controlled mainly by the polarity of the environment around CO. The C−O stretching frequency (ν_{C-O}) in *Paramecium* Hb is detected at 1974 cm^{-1} (Figure 11A), and it shifts to 1885 cm^{-1} with $^{13}C^{18}O$. The difference feature at 1861/1842 cm^{-1} (spectrum c) arises most likely from a combination band of ν_4 (1369 cm^{-1}) and ν_{Fe-CO} (493/477 cm^{-1}) (*68*) that

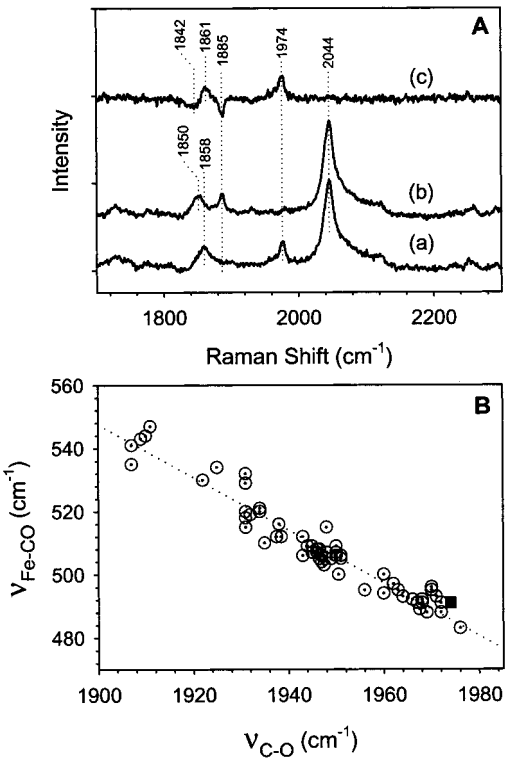

FIGURE 11: (A) Resonance Raman spectra of the carbon monoxide complex of *Paramecium* Hb in the 1700−2300 cm^{-1} region. The spectra shown are (a) with $^{12}C^{16}O$, (b) with $^{13}C^{18}O$, and (c) the $^{12}C^{16}O - {}^{13}C^{18}O$ difference. The protein is in 100 mM sodium phosphate buffer (pH 7.4). (B) Correlation between Fe−CO (ν_{Fe-CO}) and C−O (ν_{C-O}) stretching frequencies for various heme proteins that have histidine as the proximal ligand: (⊙) stretching frequencies of globins and peroxidases and (■) the frequencies of *Paramecium* HbCO.

is predicted to appear at 1862/1846 cm^{-1} for *Paramecium* HbCO. The ν_{C-O} line of *Paramecium* HbCO at 1974 cm^{-1} is close to the A_0 frequency in mutant Mbs (∼1968 cm^{-1}) containing nonpolar substitutions in the distal pocket (see ref *64*). To determine if the environmental modulations of the ν_{C-O} frequency also affect the ν_{Fe-CO} frequency, we plot ν_{C-O} versus ν_{Fe-CO} (Figure 11B). The point corresponding to *Paramecium* Hb falls on a correlation line that is characteristic for heme proteins that contain histidine as the proximal ligand.

Paramecium Hb serves as a good example of ligand-dependent conformational variation of the heme pocket and shows that the information derived from studies with one ligand cannot always be used to speculate about the properties of the other. Conformational differences between the CO and oxy complexes are also observed in the Hbs of *C. eugametos* and *Synechocystis* PCC6803 (T. K. Das et al., unpublished results). These properties of *Paramecium* Hb stand in contrast to the ligand binding properties of many Hbs in which the heme pocket conformation allows hydrogen bonding between the ligand and distal pocket residues in both the CO and oxy complexes (*11*, *15*, *60*, *64*).

Conclusions. In *Paramecium* Hb, although the bound oxygen in the closed conformation is stabilized by the distal residues, we believe this conformation is in dynamic equilibrium with an open conformation that has a high rate of oxygen dissociation. Both the oxygen combination and dissociation rates of *Paramecium* Hb appear to be well adapted to facilitate the diffusion of oxygen at the oxygen pressure encountered by the organism.

The close similarity of the oxygen kinetics of *Paramecium* Hb to those of Mb suggests that the most probable cellular function of this protozoan Hb is oxygen supply to the mitochondria of this unicellular organism (*69*) or the retention effect (*70*) in which incoming oxygen, captured by vicinal deoxy Hb, flows preferentially to the mitochondria, because the concentration gradient toward the mitochondrion is steeper than that toward the cell surface. Therefore, the function of *Paramecium* Hb is proposed to be distinct from the function of many other invertebrate Hbs that are believed to serve a variety of nontraditional roles in cellular metabolism.

REFERENCES

1. Hardison, R. (1998) Hemoglobins from bacteria to man: evolution of different patterns of gene expression, *J. Exp. Biol. 201*, 1099−1117.
2. Wittenberg, J. B., and Wittenberg, B. A. (1990) Mechanisms of cytoplasmic hemoglobin and myoglobin function, *Annu. Rev. Biophys. Biophys. Chem. 19*, 217−241.
3. Moens, L., Vanfleteren, J., Van de Peer, Y., Peeters, K., Kapp, O., Czeluzniak, J., Goodman, M., Blaxter, M., and Vinogradov, S. (1996) Globins in nonvertebrate species: dispersal by horizontal gene transfer and evolution of the structure−function relationships, *Mol. Biol. Evol. 13*, 324−333.
4. Arredondo-Peter, R., Hargrove, M. S., Moran, J. F., Sarath, G., and Klucas, R. V. (1998) Plant hemoglobins, *Plant Physiol. 118*, 1121−1125.
5. Crawford, M. J., and Goldberg, D. E. (1998) Role for the *Salmonella* flavohemoglobin in protection from nitric oxide, *J. Biol. Chem. 273*, 12543−12547.
6. Gardner, P. R., Gardner, A. M., Martin, L. A., and Salzman, A. L. (1998) Nitric oxide dioxygenase: an enzymic function for flavohemoglobin, *Proc. Natl. Acad. Sci. U.S.A. 95*, 10378−10383.
7. Minning, D. M., Gow, A. J., Bonaventura, J., Braun, R., Dewhirst, M., Goldberg, D. E., and Stamler, J. S. (1999) *Ascaris* haemoglobin is a nitric oxide-activated "deoxygenase", *Nature 401*, 497−502.
8. Membrillo-Hernandez, J., Coopamah, M. D., Anjum, M. F., Stevanin, T. M., Kelly, A., Hughes, M. N., and Poole, R. K. (1999) The flavohemoglobin of *Escherichia coli* confers resistance to a nitrosating agent, a "Nitric Oxide Releaser", and paraquat and is essential for transcriptional responses to oxidative stress, *J. Biol. Chem. 274*, 748−754.
9. Sowa, A. W., Duff, S. M. G., Guy, P. A., and Hill, R. D. (1998) Altering hemoglobin levels changes energy status in maize cells under hypoxia, *Proc. Natl. Acad. Sci. U.S.A. 95*, 10317−10321.
10. Das, T. K., Couture, M., Lee, H. C., Peisach, J., Rousseau, D. L., Wittenberg, B. A., Wittenberg, J. B., and Guertin, M. (1999) Identification of the ligands to the ferric heme of *Chlamydomonas* chloroplast hemoglobin: Evidence for ligation of tyrosine-63 (B10) to the heme, *Biochemistry 38*, 15360−15368.
11. Das, T. K., Lee, H. C., Duff, S. M. G., Hill, R. D., Peisach, J., Rousseau, D. L., Wittenberg, B. A., and Wittenberg, J. B. (1999) The heme environment in barley hemoglobin, *J. Biol. Chem. 274*, 4207−4212.
12. Couture, M., Das, T. K., Lee, H. C., Peisach, J., Rousseau, D. L., Wittenberg, B. A., Wittenberg, J. B., and Guertin, M. (1999) *Chlamydomonas* chloroplast ferrous hemoglobin. Heme pocket structure and reactions with ligands, *J. Biol. Chem. 274*, 6898−6910.
13. Das, T. K., Couture, M., Guertin, M., and Rousseau, D. L. (2000) Distal interactions in the cyanide complex of ferric *Chlamydomonas* hemoglobin, *J. Phys. Chem.* (in press).
14. Thorsteinsson, M. V., Bevan, D. R., Potts, M., Dou, Y., Eich, R. F., Hargrove, M. S., Gibson, Q. H., and Olson, J. S. (1999)

A cyanobacterial hemoglobin with unusual ligand binding kinetics and stability properties, *Biochemistry 38*, 2117−2126.
15. Das, T. K., Friedman, J. M., Kloek, A. P., Goldberg, D. E., and Rousseau, D. L. (2000) Origin of the anomalous Fe−CO stretching mode in the CO complex of *Ascaris* hemoglobin, *Biochemistry 39*, 837−842.
16. De Baere, I., Perutz, M. F., Kiger, L., Marden, M. C., and Poyart, C. (1994) Formation of two hydrogen bonds from the globin to the heme-linked oxygen molecule in *Ascaris* hemoglobin, *Proc. Natl. Acad. Sci. U.S.A. 91*, 1594−1597.
17. Kloek, A. P., Yang, J., Mathews, F. S., Frieden, C., and Goldberg, D. E. (1994) The tyrosine B10 hydroxyl is crucial for oxygen avidity of *Ascaris* hemoglobin, *J. Biol. Chem. 269*, 2377−2379.
18. Couture, M., Yeh, S. R., Wittenberg, B. A., Wittenberg, J. B., Ouellet, Y., Rousseau, D. L., and Guertin, M. (1999) A cooperative oxygen-binding hemoglobin from *Mycobacterium tuberculosis*, *Proc. Natl. Acad. Sci. U.S.A. 96*, 11223−11228.
19. Peterson, E. S., Huang, S. C., Wang, J. Q., Miller, L. M., Vidugiris, G., Kloek, A. P., Goldberg, D. E., Chance, M. R., Wittenberg, J. B., and Friedman, J. M. (1997) A comparison of functional and structural consequences of the tyrosine B10 and glutamine E7 motifs in two invertebrate hemoglobins (*Ascaris suum* and *Lucina pectinata*), *Biochemistry 36*, 13110−13121.
20. Gibson, Q. H., Regan, R., Olson, J. S., Carver, T. E., Dixon, B., Pohajdak, B., Sharma, P. K., and Vinogradov, S. N. (1993) Kinetics of ligand binding to *Pseudoterranova decipiens* and *Ascaris suum* hemoglobins and to Leu-29→Tyr sperm whale myoglobin mutant, *J. Biol. Chem. 268*, 16993−16998.
21. Kraus, D. W., and Wittenberg, J. B. (1990) Hemoglobins of the *Lucina pectinata*/bacteria symbiosis. I. Molecular properties, kinetics and equilibria of reactions with ligands, *J. Biol. Chem. 265*, 16043−16053.
22. Kraus, D. W., Wittenberg, J. B., Lu, J. F., and Peisach, J. (1990) Hemoglobins of the *Lucina pectinata*/bacteria symbiosis. II. An electron paramagnetic resonance and optical spectral study of the ferric proteins, *J. Biol. Chem. 265*, 16054−16059.
23. Pesce, A., Couture, M., Dewilde, S., Guertin, M., Yamauchi, K., Ascenzi, P., Moens, L., and Bolognesi, M. (2000) A novel two-over-two α-helical sandwich fold is characteristic of the truncated hemoglobin family, *EMBO J. 19*, 2424−2434.
24. Bolognesi, M., Bordo, D., Rizzi, M., Tarricone, C., and Ascenzi, P. (1997) Nonvertebrate hemoglobins: structural bases for reactivity, *Prog. Biophys. Mol. Biol. 68*, 29−68.
25. Yang, J., Kloek, A. P., Goldberg, D. E., and Mathews, F. S. (1995) The structure of *Ascaris* hemoglobin domain I at 2.2 Å resolution: molecular features of oxygen avidity, *Proc. Natl. Acad. Sci. U.S.A. 92*, 4224−4228.
26. Iwaasa, H., Takagi, T., and Shikama, K. (1989) Protozoan myoglobin from *Paramecium caudatum*. Its unusual amino acid sequence, *J. Mol. Biol. 208*, 355−358.
27. Yamauchi, K., Ochiai, T., and Usuki, I. (1992) The unique structure of the *Paramecium caudatum* hemoglobin gene: the presence of one intron in the middle of the coding region, *Biochim. Biophys. Acta 1171*, 81−87.
28. Yamauchi, K., Tada, H., and Usuki, I. (1995) Structure and evolution of *Paramecium* hemoglobin genes, *Biochim. Biophys. Acta 1264*, 53−62.
29. Couture, M., Chamberland, H., St-Pierre, B., Lafontaine, J., and Guertin, M. (1994) Nuclear genes encoding chloroplast hemoglobins in the unicellular green alga *Chlamydomonas eugametos*, *Mol. Gen. Genet. 243*, 185−197.
30. Ikehara, M., Ohtsuka, E., Tokunaga, T., Taniyama, Y., Iwai, S., Kitano, K., Miyamoto, S., Ohgi, T., Sakuragawa, Y., Fujiyama, K., Ikari, T., Kobayashi, M., Miyake, T., Shibahara, S., Ono, A., Ueda, T., Tanaka, T., Baba, H., Miki, T., Sakurai, A., Oishi, T., Chisaka, O., and Matsubara, K. (1984) Synthesis of a gene for human growth hormone and its expression in *Escherichia coli*, *Proc. Natl. Acad. Sci. U.S.A. 81*, 5956−5960.
31. Dewilde, S., Blaxter, M., Van Hauwaert, M. L., Van Houtte, K., Pesce, A., Griffon, N., Kiger, L., Marden, M. C., Vermeire, S., Vanfleteren, J., Esmans, E., and Moens, L. (1998) Structural, functional and genetic characterization of *Gastrophilus* hemoglobin, *J. Biol. Chem. 273*, 32467−32474.
32. Weber, R. E. (1981) Cationic control of O_2 affinity in lugworm erythrocruorin, *Nature 292*, 386−387.
33. Weber, R. E. (1992) Use of ionic and zwitterionic (Tris/BisTris and HEPES) buffers in studies on hemoglobin function, *J. Appl. Physiol. 72*, 1611−1615.
34. Duff, S. M. G., Wittenberg, J. B., and Hill, R. D. (1997) Expression, purification, and properties of recombinant barley (*Hordeum* sp.) hemoglobin. Optical spectra and reactions with gaseous ligands, *J. Biol. Chem. 272*, 16746−16752.
35. Talbot, B., Brunori, M., Antonini, E., and Wyman, J. (1971) Studies on the reaction of isocyanides with haemproteins. I. Equilibria and kinetics of the binding to the isolated chains of human haemoglobin, *J. Mol. Biol. 58*, 261−276.
36. Antonini, E., and Brunori, M. (1971) in *Hemoglobin and myoglobin in their reactions with ligands* (Neuberger, A., and Tatum, E. L., Eds.) pp 1−436, North-Holland Publishing, Amsterdam.
37. Smith, M. H., George, P., and Preer, J. R., Jr. (1962) Preliminary observations on isolated *Paramecium* hemoglobin, *Arch. Biochem. Biophys. 99*, 313−318.
38. Wang, M.-Y. R., Hoffman, B. M., Shire, S. J., and Gurd, F. R. N. (1979) Oxygen binding to myoglobins and their cobalt analogues, *J. Am. Chem. Soc. 101*, 7394−7397.
39. Hu, S., Smith, K. M., and Spiro, T. G. (1996) Assignment of protoheme resonance Raman spectrum by heme labeling in myoglobin, *J. Am. Chem. Soc. 118*, 12638−12646.
40. Yu, N.-T., and Kerr, E. A. (1988) Vibrational modes of coordinated CO, CN^-, O_2 and NO, in *Biological Application of Raman Spectroscopy* (Spiro, T. G., Ed.) Vol. 3, pp 39−95, Wiley-Interscience, New York.
41. Kitagawa, T. (1988) The heme protein structure and the iron histidine stretching mode, in *Biological Application of Raman Spectroscopy* (Spiro, T. G., Ed.) Vol. 3, pp 97−131, Wiley-Interscience, New York.
42. Rousseau, D. L., and Friedman, J. M. (1988) Transient and cryogenic studies of photodissociated hemoglobin and myoglobin, in *Biological Application of Raman Spectroscopy* (Spiro, T. G., Ed.) Vol. 3, pp 133−215, Wiley-Interscience, New York.
43. Wang, J., Caughey, W. S., and Rousseau, D. L. (1996) Resonance Raman scattering: a probe of heme protein-bound nitric oxide, in *Methods in Nitric Oxide Research* (Feelish, M., and Stamler, J. S., Eds.) pp 427−454, John Wiley and Sons Ltd., New York.
44. Argade, P. V., Sassaroli, M., Rousseau, D. L., Inubushi, T., Ikeda-Saito, M., and Lapidot, A. (1984) Confirmation of the assignment of the iron-histidine stretching mode in myoglobin, *J. Am. Chem. Soc. 106*, 6593−6596.
45. Friedman, J. M. (1994) Time-resolved resonance Raman spectroscopy as a probe of structure, dynamics and reactivity of hemoglobin, *Methods Enzymol. 232*, 205−231.
46. Das, T. K., Khan, I., Rousseau, D. L., and Friedman, J. M. (1999) Temperature-dependent quaternary state relaxation in sol−gel encapsulated hemoglobin, *Biospectroscopy 5*, S64−S70.
47. Tsubamoto, Y., Matsuoka, A., Yusa, K., and Shikama, K. (1990) Protozoan myoglobin from *Paramecium caudatum*. Its autoxidation reaction and hemichrome formation, *Eur. J. Biochem. 193*, 55−59.
48. Hirota, S., Ogura, T., Appleman, E. H., Shinzawa-Itoh, K., Yoshikawa, S., and Kitagawa, T. (1994) Observation of a new oxygen-isotope-sensitive Raman band for oxyhemoproteins and its implications in heme pocket structures, *J. Am. Chem. Soc. 116*, 10564−10570.
49. Boffi, A., Takahashi, S., Spagnuolo, C., Rousseau, D. L., and Chiancone, E. (1994) Structural characterization of oxidized dimeric *Scapharca inaequivalvis* hemoglobin by resonance Raman spectroscopy, *J. Biol. Chem. 269*, 20437−20440.
50. Rashid, A. K., and Weber, R. E. (1999) Functional differentiation in trematode hemoglobin isoforms, *Eur. J. Biochem. 260*, 717−725.

51. Terwilliger, R. C., and Read, K. R. H. (1971) Oxygen equilibrium studies of the radular muscle myoglobins of the gastropod molluscs, *Buccinum undatum* L. and *Busycon canaliculatum* L, *Int. J. Biochem. 2*, 253−261.
52. Weber, R. E., and Vinogradov, S. N. (2000) Nonvertebrate hemoglobins: functions and molecular adaptations, *Physiol. Rev.* (in press).
53. Dewilde, S., Winnepenninckx, B., Arndt, M. H. L., Nascimento, D. G., Santoro, M. M., Knight, M., Miller, A. N., Kerlavage, A. R., Geoghagen, N., Van Marck, E., Liu, L. X., Weber, R. E., Moens, L., and Arndt, M. H. (1998) Characterization of the myoglobin and its coding gene of the mollusk *Biomphalaria glabrata*, *J. Biol. Chem. 273*, 13583−13592.
54. Rashid, A. K., Van Hauwaert, M. L., Haque, M., Siddiqi, A. H., Lasters, I., De Maeyer, M., Griffon, N., Marden, M. C., Dewilde, S., Clauwaert, J., Vinogradov, S. N., and Moens, L. (1997) Trematode myoglobins, functional molecules with a distal tyrosine, *J. Biol. Chem. 272*, 2992−2999.
55. Blaxter, M. L., Vanfleteren, J. R., Xia, J., and Moens, L. (1994) Structural characterization of an *Ascaris* myoglobin, *J. Biol. Chem. 269*, 30181−30186.
56. Arredondo-Peter, R., Hargrove, M. S., Sarath, G., Moran, J. F., Lohrman, J., Olson, J. S., and Klucas, R. V. (1997) Rice hemoglobins. Gene cloning, analysis, and O_2-binding kinetics of a recombinant protein synthesized in *Escherichia coli*, *Plant Physiol. 115*, 1259−1266.
57. Friedman, J. M., Scott, T. W., Stepnoski, R. A., Ikeda-Saito, M., and Yonetani, T. (1983) The iron-proximal histidine linkage and protein control of oxygen binding in hemoglobin. A transient Raman study, *J. Biol. Chem. 258*, 10564−10572.
58. Rousseau, D. L., and Ondrias, M. R. (1983) Resonance Raman scattering studies of the quaternary structure transition in hemoglobin, *Annu. Rev. Biophys. Bioeng. 12*, 357−380.
59. Yeh, S. R., Couture, M., Ouellet, Y., Guertin, M., and Rousseau, D. L. (2000) A cooperative oxygen binding hemoglobin from *Mycobacterium tuberculosis*. Stabilization of heme ligands by a distal tyrosine residue, *J. Biol. Chem. 275*, 1679−1684.
60. Unno, M., Christian, J. F., Olson, J. S., Sage, J. T., and Champion, P. M. (1998) Evidence for hydrogen bonding effects in the iron ligand vibrations of carbonmonoxy myoglobin, *J. Am. Chem. Soc. 120*, 2670−2671.
61. Mourant, J. R., Braunstein, D. P., Chu, K., Frauenfelder, H., Nienhaus, G. U., Ormos, P., and Young, R. D. (1993) Ligand binding to heme proteins. II. Transitions in the heme pocket of myoglobin, *Biophys. J. 65*, 1496−1507.
62. Sage, J. T., Morikis, D., and Champion, P. M. (1991) Spectroscopic studies of myoglobin at low pH: heme structure and ligation, *Biochemistry 30*, 1227−1237.
63. Ramsden, J., and Spiro, T. G. (1989) Resonance Raman evidence that distal histidine protonation removes the steric hindrance to upright binding of carbon monoxide by myoglobin, *Biochemistry 28*, 3125−3128.
64. Phillips, G. N., Jr., Teodoro, M. L., Li, T., Smith, B., and Olson, J. S. (1999) Bound CO as a molecular probe of electrostatic potential in the distal pocket of myoglobin, *J. Phys. Chem. B 103*, 8817−8829.
65. Ray, G. B., Li, X.-Y., Ibers, J. A., Sessler, J. L., and Spiro, T. G. (1994) How far can proteins bend the FeCO unit? Distal polar and steric effects in heme proteins and models, *J. Am. Chem. Soc. 116*, 162−176.
66. Park, K. D., Guo, K., Adebodun, F., Chiu, M. L., Sligar, S. G., and Oldfield, E. (1991) Distal and proximal ligand interactions in heme proteins: correlations between C−O and Fe−C vibrational frequencies, oxygen-17 and carbon-13 nuclear magnetic resonance chemical shifts, and oxygen-17 nuclear quadrupole coupling constants in $C^{17}O$- and ^{13}CO-labeled species, *Biochemistry 30*, 2333−2347.
67. Ling, J., Li, T., Olson, J. S., and Bocian, D. F. (1994) Identification of the iron−carbonyl stretch in distal histidine mutants of carbonmonoxymyoglobin, *Biochim. Biophys. Acta 1188*, 417−421.
68. Wang, J., Takahashi, S., and Rousseau, D. L. (1995) Identification of the overtone of the Fe−CO stretching mode in heme proteins: a probe of the heme active site, *Proc. Natl. Acad. Sci. U.S.A. 92*, 9402−9406.
69. Wittenberg, J. B. (1992) Functions of cytoplasmic hemoglobins and myohemerythrin, in *Advances in Comparative and Environmental Physiology* (Mangum, C. P., Ed.) Vol. 13, Chapter 3, pp 59−85, Springer-Verlag, New York.
70. Silhavy, T. J., Szmelcman, S., Boos, W., and Schwartz, M. (1975) On the significance of the retention of ligand by protein, *Proc. Natl. Acad. Sci. U.S.A. 72*, 2120−2124.
71. Gibson, Q. H., and Smith, M. H. (1965) Rates of reaction of *Ascaris* haemoglobins with ligands, *Proc. R. Soc. London, Ser. B. 163*, 206−214.
72. Gibson, Q. H., Wittenberg, J. B., Wittenberg, B. A., Bogusz, D., and Appleby, C. A. (1989) The kinetics of ligand binding to plant hemoglobins. Structural implications, *J. Biol. Chem. 264*, 100−107.
73. Springer, B. A., Egeberg, K. D., Sligar, S. G., Rohlfs, R. J., Mathews, A. J., and Olson, J. S. (1989) Discrimination between oxygen and carbon monoxide and inhibition of autooxidation by myoglobin. Site-directed mutagenesis of the distal histidine, *J. Biol. Chem. 264*, 3057−3060.
74. Olson, J. S., Mathews, A. J., Rohlfs, R. J., Springer, B. A., Egeberg, K. D., Sligar, S. G., Tame, J., Renaud, J. P., and Nagai, K. (1988) The role of the distal histidine in myoglobin and haemoglobin, *Nature 336*, 265−266.
75. Kiger, L., Rashid, A. K., Griffon, N., Haque, M., Moens, L., Gibson, Q. H., Poyart, C., and Marden, M. C. (1998) Trematode hemoglobins show exceptionally high oxygen affinity, *Biophys. J. 75*, 990−998.
76. Trevaskis, B., Watts, R. A., Andersson, C. R., Llewellyn, D. J., Hargrove, M. S., Olson, J. S., Dennis, E. S., and Peacock, W. J. (1997) Two hemoglobin genes in *Arabidopsis thaliana*: the evolutionary origins of leghemoglobins, *Proc. Natl. Acad. Sci. U.S.A. 94*, 12230−12234.

BI001681D